crystals

MDPI

Article

One-Pot Synthesis, X-ray Single Crystal and Molecular Insight of Enaminone-Based β-Morpholino-/*N*-Methylpiperazinyl-/Pyrrolidinylpropiophenone

Assem Barakat [1,2,*], Saied M. Soliman [2], Matti Haukka [3], Abdullah Mohammed Al-Majid [1], Mohammad Shahidul Islam [1], M. Ali [1] and Mohammed Rafi Shaik [1]

1 Department of Chemistry, College of Science, King Saud University, P. O. Box 2455, Riyadh 11451, Saudi Arabia; amajid@ksu.edu.sa (A.M.A.-M.); mislam@ksu.edu.sa (M.S.I.); maly.c@ksu.edu.sa (M.A.); mrshaik@ksu.edu.sa (M.R.S.)

2 Department of Chemistry, Faculty of Science, Alexandria University, P.O. Box 426, Ibrahimia, Alexandria 21321, Egypt; saied1soliman@yahoo.com

3 Department of Chemistry, University of Jyväskylä, P.O. Box 35, FI-40014 Jyväskylä, Finland; matti.o.haukka@jyu.fi

* Correspondence: ambarakat@ksu.edu.sa; Tel.: +966-11467-5901; Fax: +966-11467-5992

Received: 20 March 2020; Accepted: 4 April 2020; Published: 8 April 2020

Abstract: One-pot synthesis of three enaminones, (*E*)-1-(4-chlorophenyl)-3-morpholinoprop-2-en-1-one **1**, (*E*)-1-(4-chlorophenyl)-3-(4-methylpiperazin-1-yl)prop-2-en-1-one **2**, and (*E*)-1-(4-chlorophenyl)-3-(pyrrolidin-1-yl)prop-2-en-1-one **3** were achieved. The synthetic protocol *via* three components reaction of *p*-chloroacetophenone with DMFDMA (*N*,*N*-dimethylformamid-dimethylacetal) and the corresponding secondary amines (morpholine/*N*-methylpiperazine/pyrrolidine) in dioxane under heating for 2.5–4 h at 102 °C yielded the requisite enaminones. This protocol has the advantage of no separation of intermediate, no need for column purification with quantitative yield for the target compounds. The chemical features of the β-enaminones **1**–**3** were assigned by NMR. β-Enaminones **1**, and **2** were assigned by single crystal X-ray diffraction technique. The intermolecular interactions in the crystal structures were analyzed quantitatively using Hirshfeld analysis. The Cl ... H and O ... H hydrogen bonds are common in both compounds while the C-H ... π and N ... H contacts are more significant in **2** than **1**. DFT studies were investigated to show the electronic and spectroscopic properties (NMR and UV-Vis) of the studied systems.

Keywords: β-enaminone; DMFDMA; morpholine; *N*-methylpiperazine; pyrrolidine; Hirshfeld analysis

1. Introduction

β-Enaminones are an important building block for the synthesis of many compounds which have pharmacological features including antitumor [1,2], anti-inflammatory [3], anti-epileptic [4], anticonvulsant [5], antibacterial [6] and other therapeutic agents [7–9]. Some of the reported heterocycles which β-enaminones were utilized as precursors in the synthetic routes of pharmacologically active precursors such as pyrazoles, pyridinones, dibenzodiazepines, quinolines, oxazoles and tetrahydrobenzoxazines [10–14].

Many synthetic routes have been used for the synthesis of this special scaffold. Several catalysts such as $InBr_3$ [15], vanadium (IV) acetylacetonate [16], $LaCl_3$ [17], (CuI–2,2′-bipyridine–NaO*t*Bu) [18], silica supported $Fe(HSO_4)_3$ under solvent free conditions [19], silver nanoparticles [20], and bimetallic Ag–Cu alloy nanoparticles [21], etc. have all been employed in direct synthetic methods of the

β-dicarbonyl synthon with an amine to yield the β-enaminone. However, these reported protocols have been shown to have disadvantages, including low chemical yield, longer reaction time, complication in the reaction work-up with low selectivity and no generality. Therefore, a simple, direct and efficient synthetic route with a high chemical yield for β-enaminones is highly demanded. In this study, we describe a one-pot direct method with high efficiency for β-enaminone synthesis via reaction of acetophenone with DMFDMA and three different secondary amines. Analyses of the single crystal structures of the two final products were conducted by X-ray diffraction techniques. Hirshfeld analysis, DFT calculations, UV-Vis spectral assignments are also presented.

2. Materials and Methods

UV analyses were carried out on a PerkinElmer lambda 35 spectrophotometer (Waltham, MA, USA). The ^{1}H NMR and ^{13}C-NMR spectra of both β-enaminones were recorded on a JEOL 400-MHz spectrometer (JEOL, Ltd., Tokyo, Japan) at ambient temperature. The solvent used was DMSO-d_6; the chemical shifts (δ) are given in ppm. Single-crystal X-ray data of compounds **1** and **2** were collected on a Bruker Kappa APEX II diffractometer at 170 K. The crystallographic details are provided as supplementary material. The Crystal Explorer 17.5 program was used for the Hirshfeld analysis [22].

2.1. Synthesis of the Enaminones **1–3**

A mixture of *p*-Cl-acetophenone (4 mmol, 616 mg), DMF-DMA (4.8 mmol, 571 mg), morpholine (20 mmol, 1.74 gm) or *N*-methylpiperazine (20 mmol, 2.002 gm), or pyrrolidine (20 mmol, 1.72 gm) in 50 mL dioxane at 102 °C. The reaction mixture stirred under nitrogen atmosphere for 2.5–4 h. The reaction progress was checked by TLC. The solvent was removed under reduced pressure. Enaminones were obtained initially as semisolids; upon standing, they yielded solidified products. No further purification was required unless they were washed with hexane to get rid of excess amines [23].

(*E*)-1-(4-Chlorophenyl)-3-morpholinoprop-2-en-1-one **1**

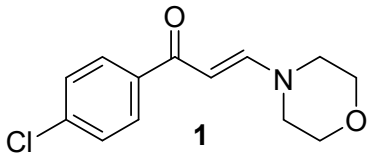

1

^{1}H-NMR (DMSO-d_6, 400 MHz) δ7.93 (d, J = 8.8 Hz, 2H), 7.71 (d, J = 12.4 Hz, 1H), 7.49 (d, J = 8.8 Hz, 2H), 6.08 (d, J = 12.4 Hz, 1H), 3.65 (t, J = 4.4 Hz, 4H), 3.46 (brs, 4H) ppm. ^{13}C-NMR (DMSO-d_6, 100 MHz) δ 184.84, 153.20, 138.65, 135.70, 129.21, 128.21, 90.84, 66.09 ppm.

(*E*)-1-(4-Chlorophenyl)-3-(4-methylpiperazin-1-yl)prop-2-en-1-one **2**

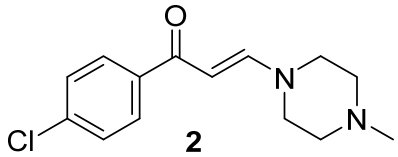

2

^{1}H-NMR (DMSO-d_6, 400 MHz) δ 7.84 (d, J = 8.8 Hz, 2H), 7.61 (d, J = 12.4 Hz, 1H), 7.40 (d, J = 8.8 Hz, 2H), 5.97 (d, J = 12.4 Hz, 1H), 3.26 (s, 3H), 2.27 (t, J = 4.4 Hz, 4H), 2.11 (brs, 4H) ppm. ^{13}C-NMR (DMSO-d_6, 100 MHz) δ 184.75, 153.04, 138.75, 135.61, 129.13, 128.17, 90.57, 55.07, 53.65, 45.57 ppm.

(*E*)-1-(4-Chlorophenyl)-3-(pyrrolidin-1-yl)prop-2-en-1-one **3**

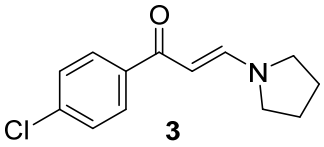

3

^{1}H-NMR (DMSO-d_6, 400 MHz) δ 7.90 (d, J = 3.8Hz, 3H), 7.49 (d, J = 8.08 Hz, 1H), 7.40 (d, J = 8.8 Hz, 2H), 5.73 (d, J = 11.96 Hz, 1H), 3.56 (t, J = 6.68 Hz, 2H), 3.25 (t, J = 6.84Hz, 2H), 1.96 (m, 2H), 1.84 (m, 2H) ppm. ^{13}C-NMR (DMSO-d_6, 100 MHz) δ 184.62, 150.69, 139.51, 136.03, 129.61, 128.77, 92.11, 52.58, 47.50, 25.36 ppm.

2.2. Computational Methods

All DFT calculations were performed using the Gaussian 09 software package [24] utilizing B3LYP/6-31G(d,p) method. The optimized structures showed no imaginary frequencies and were used to predict the electronic and spectroscopic properties of the studied molecules. Natural population analysis was performed using the NBO 3.1 program as implemented in the Gaussian 09W package [25]. The self-consistent reaction field (SCRF) method [26,27] was used to model the solvent effects when calculated the optimized geometries in solution.

3. Results and Discussion

3.1. Synthesis of Enaminones **1–3**

The three targeted β-enaminones **1–3** were synthesized *via* an efficient one-pot direct method as shown in Scheme 1. The synthetic protocol *via* reaction of *p*-chloroacetophenone with DMFDMA and the corresponding secondary amines (morpholine/*N*-methylpiperazine and pyrrolidine) in dioxane was used under heating for 2.5–4 h at 102 °C to yield the requisite enaminones. The chemical features of the three synthesized β-enaminones were well-assigned; the spectral data of the enaminones **1**, and **2** fit with the reported literature [28]. Additionally, X-ray single crystal (Figure 1), Hirshfeld and DFT calculations were conducted to confirm molecular structural aspects of the compounds **1**, and **2**. The chemical structure of Enaminone **3** was confirmed by ^{1}H-NMR as follows: two aromatic and one olefinic protons appeared at δ 7.90 ppm; two aromatic protons at δ 7.49; a second olefinic proton appeared at 5.73 ppm; eight protons of the pyrrolidine ring appeared as follows: four protons close to nitrogen at δ 3.56 and 3.25 ppm; finally, the second four protons appeared as multiplet at δ 1.96, and 1.84 ppm. ^{13}C-NMR spectrum were constituent with proposed structure (see supplementary information).

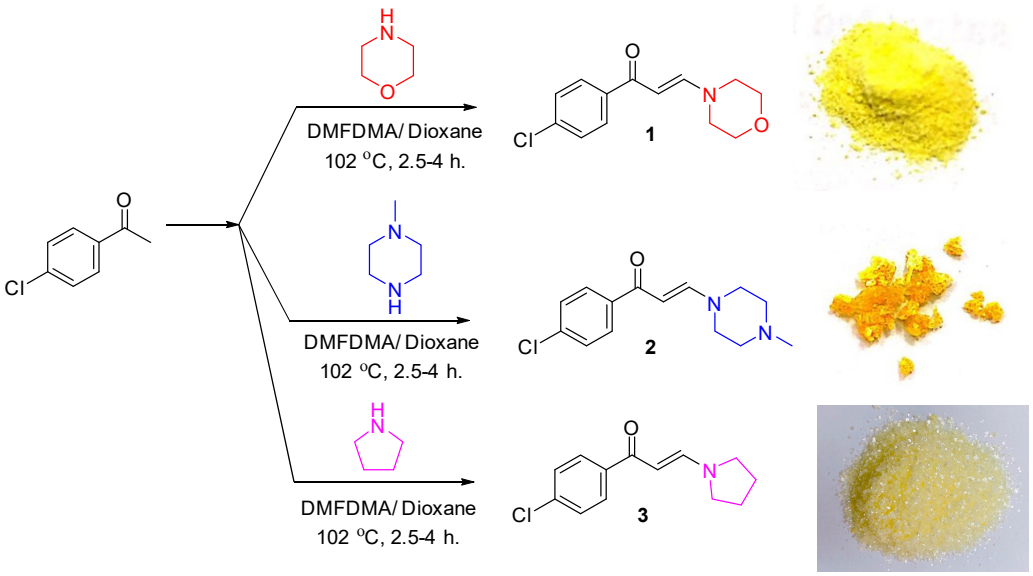

Scheme 1. Synthesis of β-enaminone **1–3**.

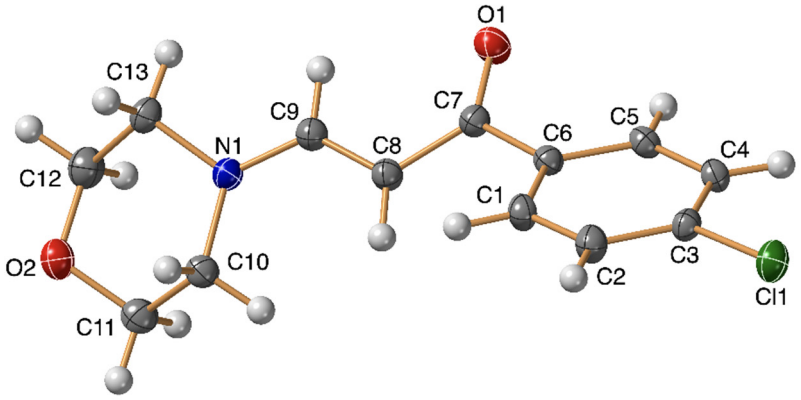

(**a**)

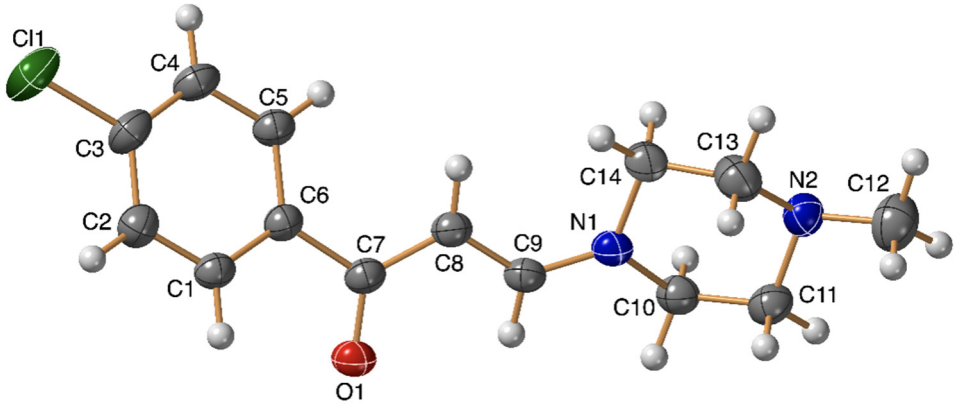

(**b**)

Figure 1. X-ray structure of **1** (**a**), and **2** (**b**). Thermal ellipsoids were drawn at 50% probability level.

3.2. *X-ray Structure of* **1**, *and* **2**

The structure of **1** was revealed as an inversion twin in a chiral space group $P2_12_12_1$. The structure of **2** was revealed in a centrosymmetric space group $P2_1/c$. Changing the morpholine moiety of **1** to piperazine in **2** led to slight shortening of the N1-C9 distance from 1.338(2) Å to 1.328(2) Å (Table 1). Also, the C7-C8 distance was slightly shorter in the case of **2** (1.429(2) Å) than in **1** (1.442(2) Å). The changes in N1-C9 and C7-C8 bond distances were probably due to packing effects. Selected bond lengths [Å] and angles [°] for **1** and **2** are listed in Tables 1 and 2.

Table 1. Selected bond lengths [Å] and angles [°] for **1**.

Bond	Distance
Cl(1)-C(3)	1.7466(15)
O(1)-C(7)	1.2403(19)
O(2)-C(12)	1.421(2)
O(2)-C(11)	1.422(2)
N(1)-C(9)	1.338(2)
N(1)-C(10)	1.460(2)
N(1)-C(13)	1.462(2)

Table 2. Selected bond lengths [Å] and angles [°] for **2**.

Bonds	Angles
Cl(1)-C(3)	1.7427(17)
O(1)-C(7)	1.2419(19)
N(1)-C(9)	1.328(2)
N(1)-C(10)	1.460(2)
N(1)-C(14)	1.462(2)
N(2)-C(13)	1.450(2)
N(2)-C(11)	1.458(2)
N(2)-C(12)	1.460(2)

3.3. Analysis of Molecular Packing

The most important contacts and their percentages for **1**, and **2** are shown in Figure 2. The Hirshfeld surfaces are shown in Figures 3 and 4, respectively. The results indicate that the molecular units were mainly packed by the nonpolar H … H interactions, which contributed by 43.2 and 46.5% for **1**, and **2**, respectively. In case of the former, there were four red spots in the d_{norm} map corresponding to the intermolecular contacts with shorter contact distances than the van der Waals (vdW) radii sum; half of them were for the O … H hydrogen bonds that appeared as intense red circles, while the other half which appear as small fad red circles corresponding to the Cl … H hydrogen bonds. The O … H (15.5%) and Cl … H (16.2%) contact distances are 2.275 (O1 … H14) and 2.788 Å (Cl1 … H5), respectively (Figure 5). The rest of the observed contacts had either longer—or almost equal interaction—distances compared to the vdW radii sum of the elements involved in the interactions.

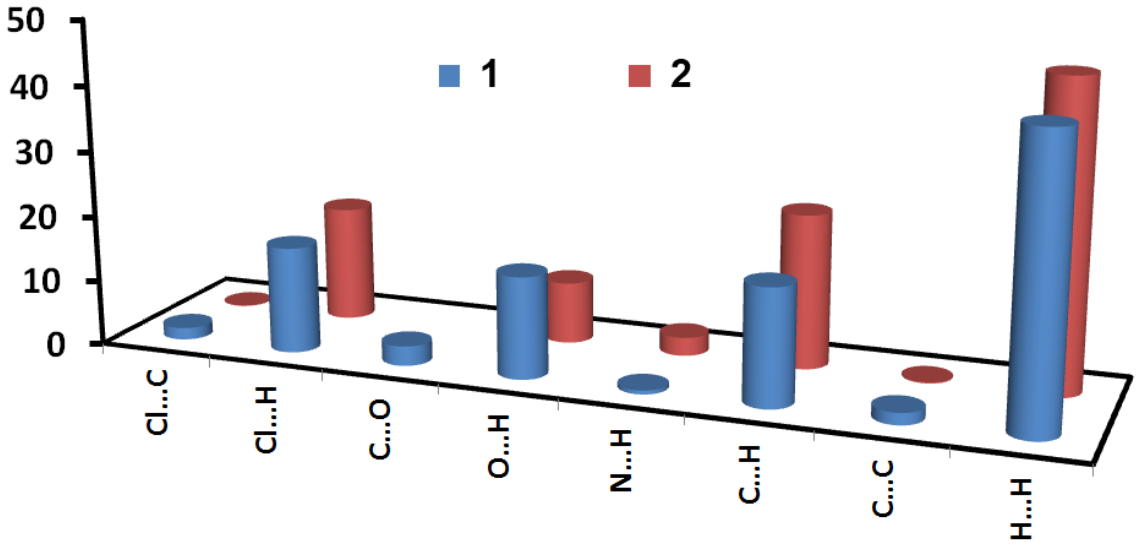

Figure 2. Percentages of intermolecular interactions in compounds **1**, and **2**.

Figure 3. *Cont.*

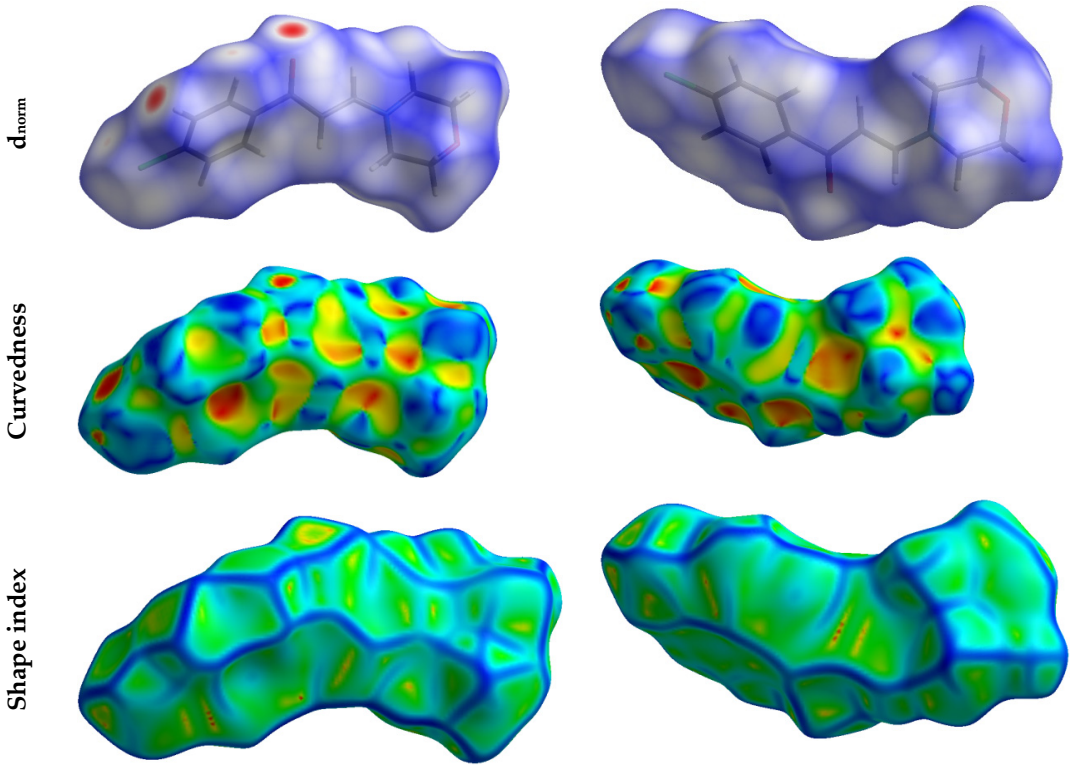

Figure 3. Hirshfeld surfaces of compound **1**.

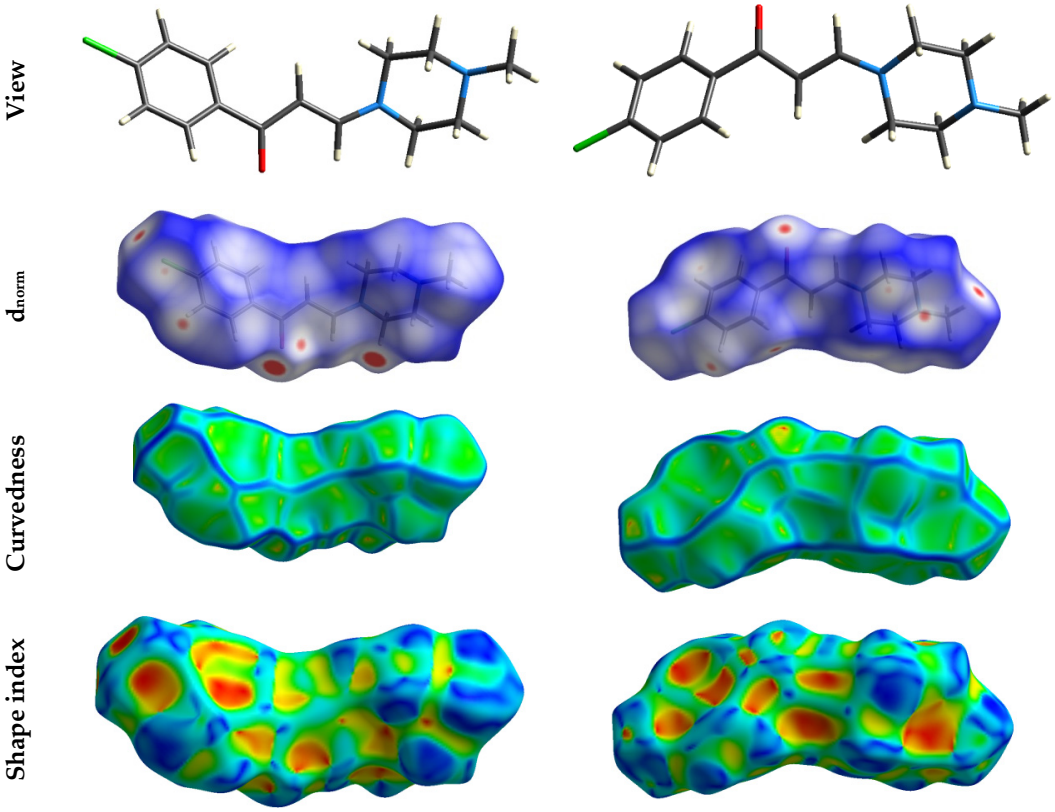

Figure 4. Hirshfeld surfaces of compound **2**.

In case of **2**, there are two Cl … H hydrogen bonds with contact distances ranges from 2.706 Å (Cl1 … H12C) to 2.802 (Cl1 … H10A) occurred between the Cl atom and the C-H protons in the

morpholine moiety from adjacent molecule. The overall Cl...H hydrogen bond contacts contributed by 17.6%. On other hand, the Hirshfeld analysis detected four potential O … H hydrogen bond contacts which were O1 … H10B (2.293 Å), O1 … H5 (2.483 Å), O1 … H4 (2.523 Å) and O1 … H9 (2.573 Å), in addition to one N2 … H2A (2.547 Å) hydrogen bond which contributed by 9.4% and 2.8%, respectively. In addition, the Hirshfeld analysis showed the presence of weak C-H … π (23.4%) interactions with C2 … H14B distance of 2.746 Å in **2** which was found less important in **1**. An illustration of the most important contacts in **2** is shown in Figures 6 and 7.

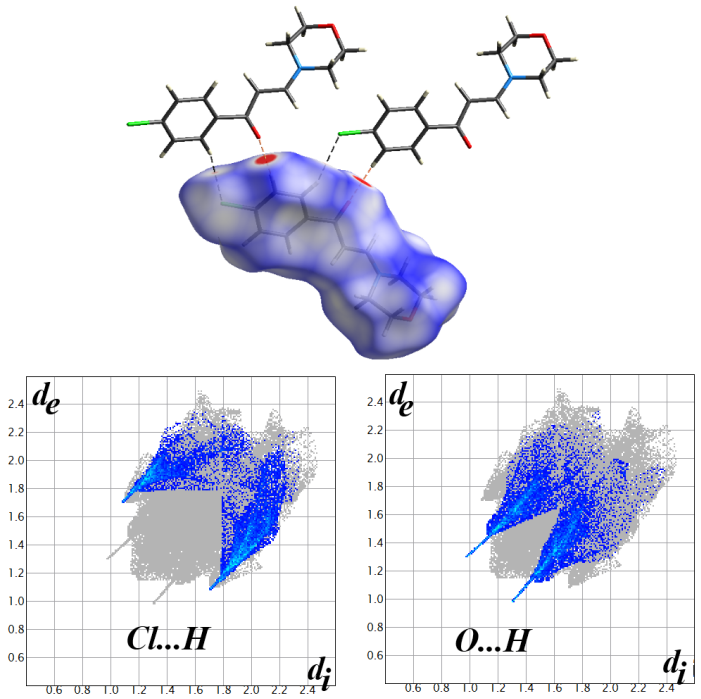

Figure 5. Fingerprint (**lower**) and d_{norm} map (**upper**) of the polar contacts in compound **1**.

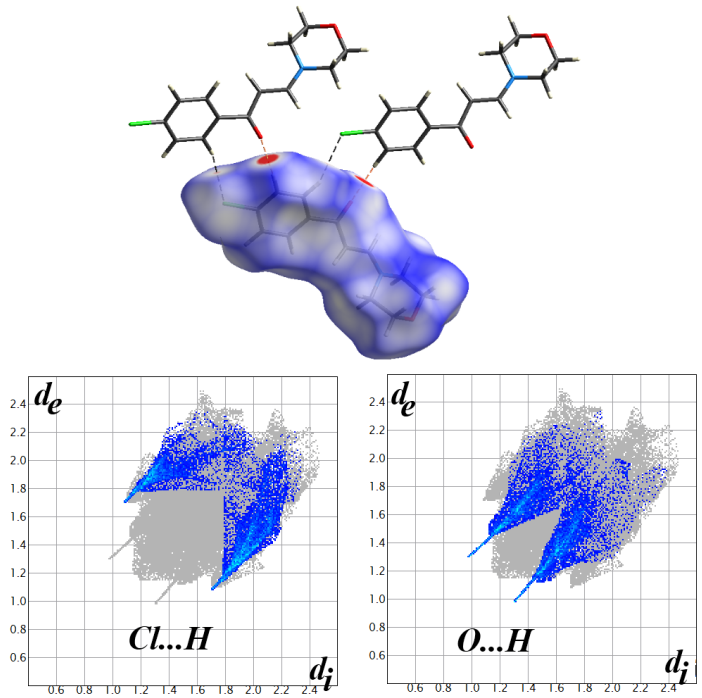

Figure 6. The fingerprint (**lower**) and d_{norm} map (**upper**) of the polar contacts in compound **2**.

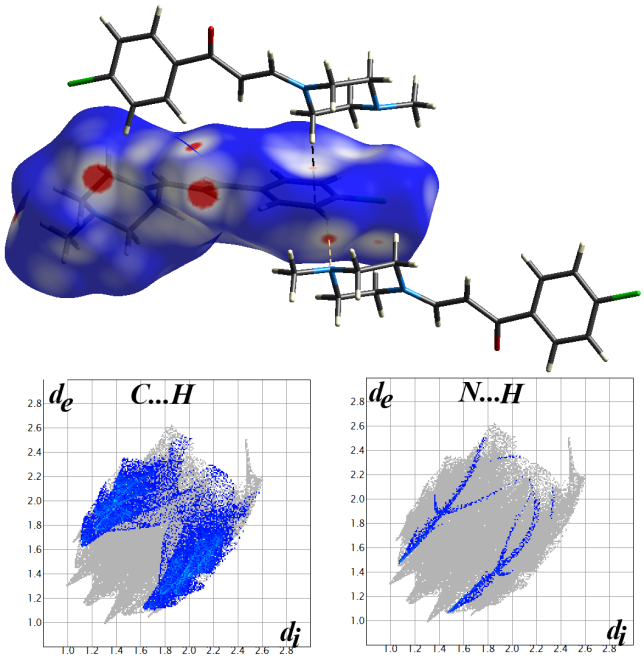

Figure 7. The fingerprint (**lower**) and d_{norm} map (**upper**) of the C ... H and N ... H contacts in compound **2**.

3.4. DFT Studies

Geometric Parameters

The optimized molecular geometries of **1**, and **2** are shown in Figure 8 (upper part) and the structure matches between the calculated and optimized structures are shown in the same figure (lower part). The calculated geometric parameters along with the experimental X-ray values are given in Table S12 (Supplementary data), while the correlation graphs between the calculated and experimental parameters are presented in Figure 9. It is clear that the experimental and calculated values are well-correlated, with correlation coefficients very close to 1. The calculated dipole moments of compound **1**, and compound **2** were 4.7665 and 6.4517 Debye, respectively, indicating the higher polarity of the latter compared to the former. The orientation of the dipole moment vector over the molecular electrostatic potential (MEP) map shown in Figure 10 was oriented towards the carbonyl oxygen atom which has the highest negative charge (Table S13 Supplementary data).

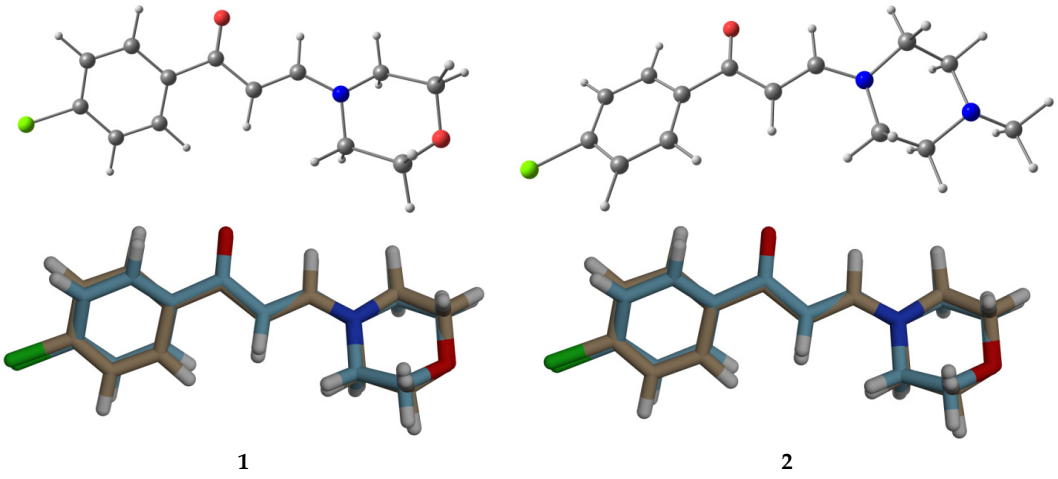

Figure 8. Optimized geometry (**upper**), and optimized/calculated structures overlay (**lower**) for compounds **1**, and **2**.

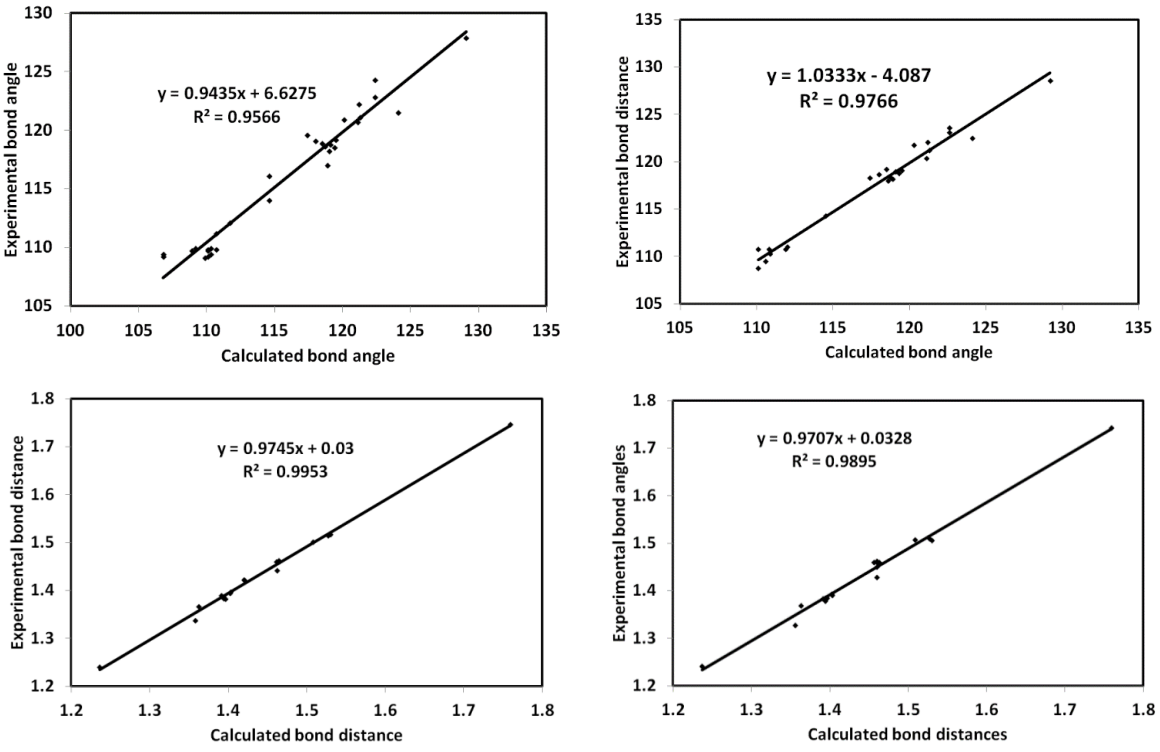

Figure 9. Correlation graphs between the calculated and experimental geometric parameters for the studied compounds **1**, and **2**.

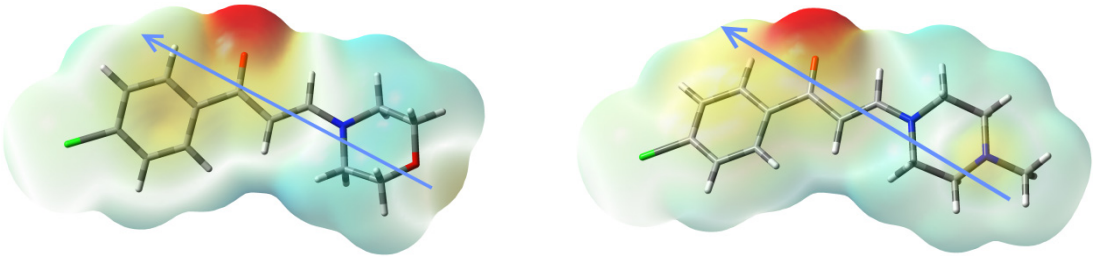

Figure 10. The MEP map and the dipole moment vector of the studied compounds **1**, and **2**. The color index from turquoise to yellow to red indicated the more negative electron density.

3.5. Reactivity Studies

The ionization potential (I), electron affinity (A), chemical potential (μ), hardness (η) as well as electrophilicity index (ω) were calculated using Equations (1)–(5) (Table 3). These parameters were employed to explain the bio-reactivity of chemical compounds [29–35].

$$I = -E_{HOMO} \quad (1)$$

$$A = -E_{LUMO} \quad (2)$$

$$\eta = (I - A)/2 \quad (3)$$

$$\mu = -(I + A)/2 \quad (4)$$

$$\omega = \mu^2/2\eta \quad (5)$$

Table 3. The calculated descriptors of compound **1**, and compound **2**.

Parameter	1	2
HOMO	−5.7664	−5.6412
LUMO	−1.4368	−1.3339
I	5.7664	5.6412
A	1.4368	1.3339
η	4.3296	4.3073
μ	−3.6016	−3.4876
ω	1.4980	1.4119

The ionization potential (I), electron affinity (A), hardness (η) as well as electrophilicity index (ω) were higher for compound **1** than compound **2,** while the opposite was true regarding the chemical potential (μ). Since the former has lower energy LUMO than the latter so; it could be expected that **1** is better electron acceptor than compound **2**. In contrast, the HOMO energy was higher for compound **2** than compound **1,** indicating that the former is better electron donor than the latter.

3.6. NMR and UV-Vis Electronic Spectra

The calculated ^{1}H and ^{13}C NMR chemical shifts using GIAO method [36] applying the PCM solvent (DMSO) model are listed in Table S14 (Supplementary data) and compared with the experimentally observed spectral shifts in the same solvent. It clear that the experimental chemical shifts are well-correlated with the calculated values, as can be seen from Figure 11 where good straight-line correlations were obtained with very good correlation coefficients of 0.9098–0.9919 and 0.9811–0.9958 for the ^{1}H and ^{13}C NMR chemical shifts, respectively.

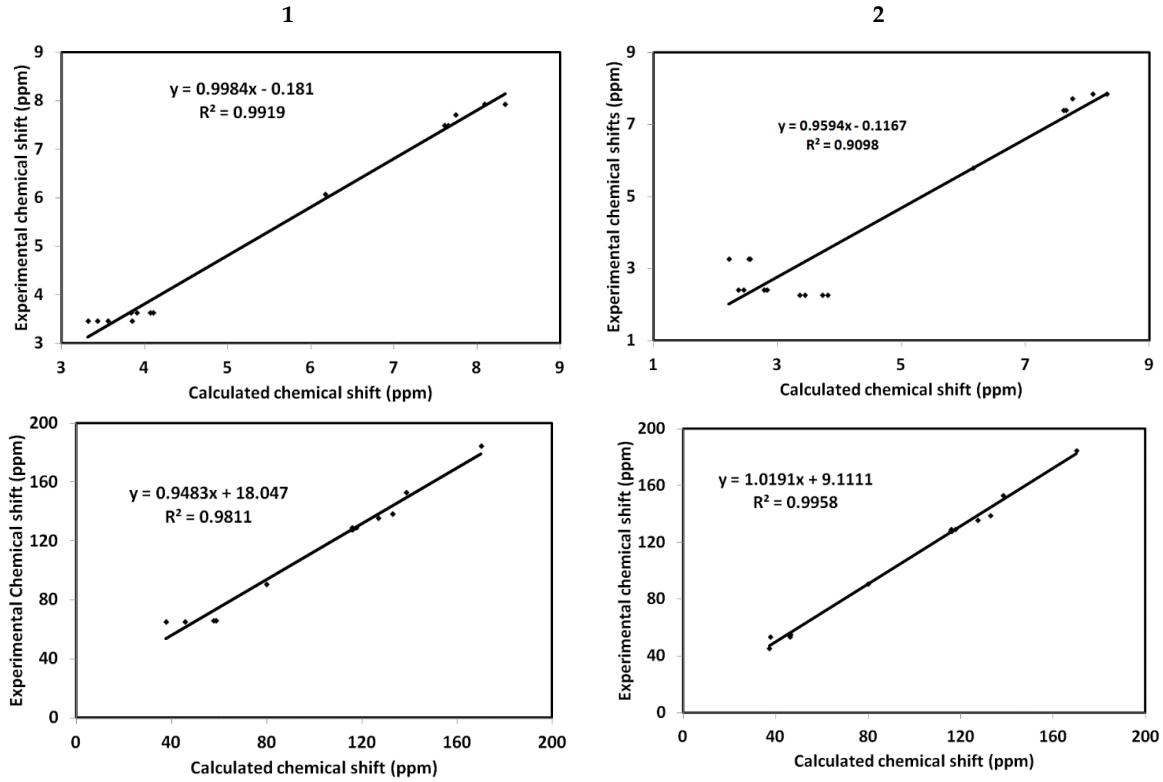

Figure 11. Correlation between calculated and experimental ^{1}H (**upper**) and ^{13}C (**lower**) NMR chemical shifts for compounds **1** (**left**), and **2** (**right**).

The experimental UV-V electronic spectra of the studied compounds **1**, and **2** are shown in Figure 12. The electronic spectra of both compounds were very similar where both compounds showed

three well-separated bands at 205, 253 and 348 nm. Theoretically, these bands were calculated and the results along with their assignments were collected in Table 4 and shown in Figure 12. The longest wavelength band was calculated at 327 nm for both compounds. This band was mainly due to the HOMO→LUMO excitation. Presentation of the HOMO and LUMO demands are shown in Figure 13 which indicated that this band may be assigned mainly as π-π* transition.

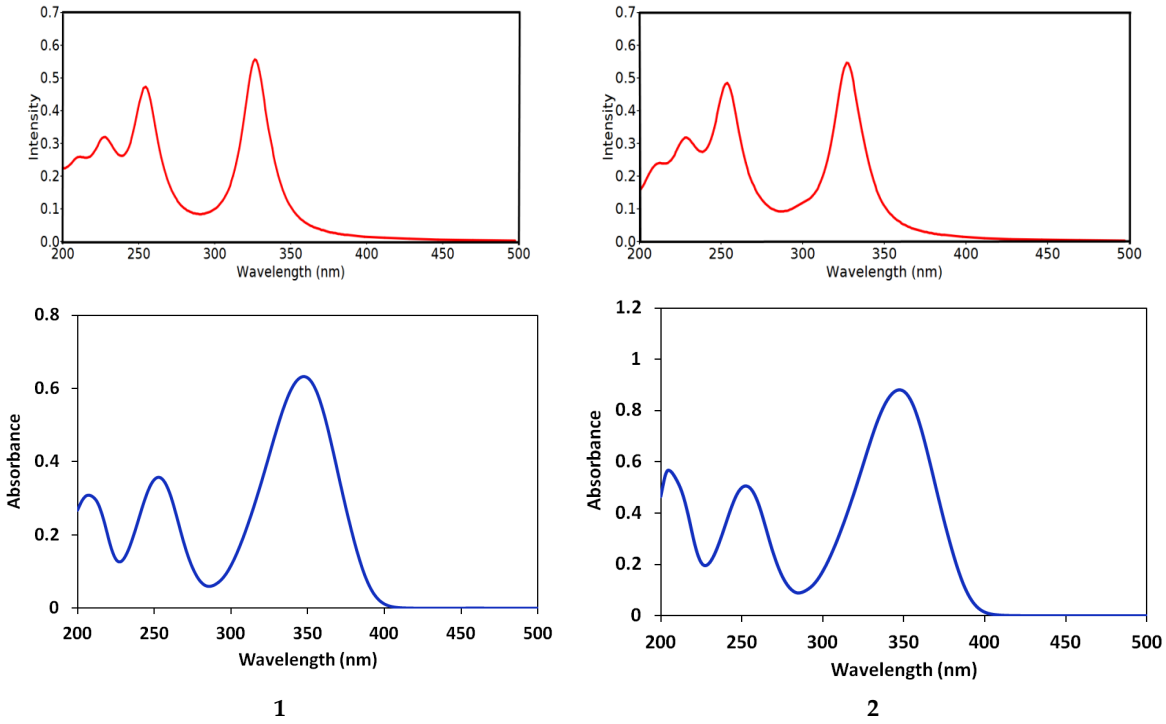

Figure 12. The experimental (blue) and calculated (red) UV-Vis electronic spectra of compounds **1**, and **2**.

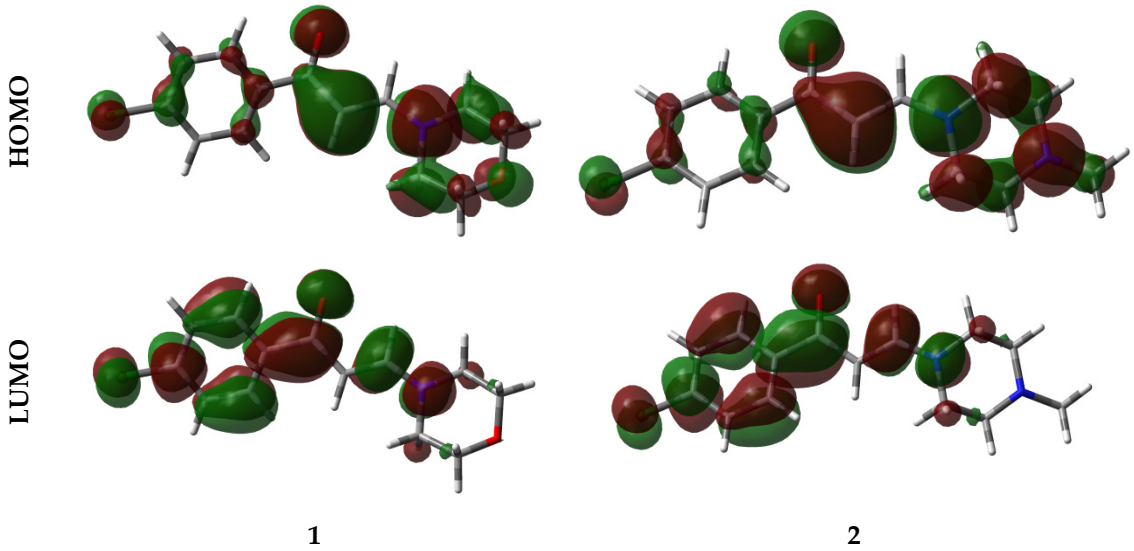

Figure 13. HOMO and LUMO levels of compounds **1**, and **2**.

Table 4. The calculated electronic transition bands (λ in nm) and their oscillator strength (f) of the studied compounds **1** and **2**.

1			**2**		
Λ	**f**	**Major Contributions**	**λ**	**F**	**Major Contributions**
326.5	0.520	HOMO→LUMO (82%), H-1→LUMO (16%)	327.0	0.500	HOMO→LUMO (79%), H-2→LUMO (19%)
254.8	0.402	H-2→LUMO (83%)	270.3	0.014	HOMO→L + 1 (94%)
209.9	0.116	H-3→LUMO (18%), H-3→L + 2 (17%), H-2→L + 1 (54%)	212.9	0.006	H-1→L + 2 (54%), HOMO→L + 3 (42%)

4. Conclusions

Three enaminones were synthesized *via* one-pot reaction. The presented protocol has the advantage of high chemical yield, mild conditions and high purity of the products with almost no cost for purification. Hirshfeld analysis of molecular packing was used for molecular-packing quantitative analysis. Also, DFT calculations were used to optimize the structure of the studied systems and predict the NMR chemical shifts, as well as the electronic molecular spectra of both systems. The substrate scope and the utility of these enaminones as building blocks under investigation in our laboratory.

Supplementary Materials: The following are available online at http://www.mdpi.com/2073-4352/10/4/282/s1. Software for X-ray determination (Tables for X-ray data); tables for computational studies; along with copies of NMR spectrum of the synthesized compounds.

Author Contributions: Conceptualization, A.B.; data curation, S.M.S. and M.H.; formal analysis, M.H., M.A. and M.R.S.; funding acquisition, A.B.; investigation, M.S.I.; methodology, M.S.I. and M.A.; software, S.M.S. and M.H.; validation, A.M.A.-M.; Visualization, A.M.A.-M.; writing—original draft, A.B. and S.M.S.; writing—review & editing, A.B. and S.M.S. All authors have read and agreed to the published version of the manuscript.

Funding: This research was funded by Project Number (RSP-2019/64), King Saud University, Riyadh, Saudi Arabia.

Acknowledgments: The authors would like to extend their sincere appreciation to Researchers Supporting Project Number (RSP-2019/64), King Saud University, Riyadh, Saudi Arabia.

Conflicts of Interest: The authors declare no conflict of interest.

References

1. Riyadh, S.M. Enaminones as building blocks for the synthesis of substituted pyrazoles with antitumor and antimicrobial activities. *Molecules* **2011**, *16*, 1834–1853. [CrossRef]
2. Ramadan, S.K.; Shaban, S.S.; Hashem, A.I. Facile and expedient synthesis and anti-proliferative activity of diversely pyrrolones bearing 1, 3-diphenylpyrazole moiety. *Synth. Commun.* **2020**, *50*, 185–196. [CrossRef]
3. Dannhardt, G.; Bauer, A.; Nowe, U. Non-Steroidal Anti-Inflammatory Agents, Part 24 [1] Pyrrolidino Enaminones as Models to Mimic Arachidonic Acid. *Archiv der Pharmazie* **1997**, *330*, 74–82. [CrossRef]
4. Khurana, M.; Salama, N.N.; Scott, K.R.; Nemieboka, N.N.; Bauer, K.S.; Eddington, N.D. Preclinical evaluation of the pharmacokinetics, brain uptake and metabolism of E121, an antiepileptic enaminone ester, in rats. *Biopharm. Drug Dispos.* **2003**, *24*, 397–407. [CrossRef]
5. Edafiogho, I.O.; Ananthalakshmi, K.V.V.; Kombian, S.B. Anticonvulsant evaluation and mechanism of action of benzylamino enaminones. *Bioorg. Med. Chem.* **2006**, *14*, 5266–5272. [CrossRef]
6. Michael, J.P.; De Koning, C.B.; Hosken, G.D.; Stanbury, T.V. Reformatsky reactions with N-arylpyrrolidine-2-thiones: Synthesis of tricyclic analogues of quinolone antibacterial agents. *Tetrahedron* **2001**, *57*, 9635–9648. [CrossRef]
7. El-Borai, M.A.; Rizk, H.F.; Beltagy, D.M.; El-Deeb, I.Y. Microwave-Assisted synthesis of some new pyrazolopyridines and their antioxidant, antitumor and antimicrobial activities. *Eur. J. Med. Chem.* **2013**, *66*, 415–422. [CrossRef]

8. Eldehna, W.M.; Abo-Ashour, M.F.; Berrino, E.; Vullo, D.; Ghabbour, H.A.; Al-Rashood, S.T.; Hassan, G.S.; Alkahtani, H.M.; Almehizia, A.A.; Alharbi, A.; et al. SLC-0111 enaminone analogs, 3/4-(3-aryl-3-oxopropenyl) aminobenzenesulfonamides, as novel selective subnanomolar inhibitors of the tumor-associated carbonic anhydrase isoform IX. *Bioorg. Chem.* **2019**, *83*, 549–558. [CrossRef]
9. Ali, M.; Barakat, A.; El-Faham, A.; Al-Rasheed, H.H.; Dahlous, K.; Al-Majid, A.M.; Sharma, A.; Yousuf, S.; Sanam, M.; Ul-Haq, Z.; et al. Synthesis and characterisation of thiobarbituric acid enamine derivatives, and evaluation of their α-glucosidase inhibitory and anti-glycation activity. *Enzyme Inhib. Med. Chem.* **2020**, *35*, 692–701. [CrossRef]
10. Chaaban, I.; Greenhill, J.V.; Akhtar, P. Enaminones in the mannich reaction. Part 2. Further investigations of internal mannich reactions. *J. Chem. Soc. Perkin Trans. 1* **1979**, *6*, 1593–1596. [CrossRef]
11. Michael, J.P.; De Koning, C.B.; Gravestock, D.; Hosken, G.D.; Howard, A.S.; Jungmann, C.M.; Krause, R.; Parsons, A.S.; Pelly, S.; Stanbury, T. Enaminones: Versatile intermediates for natural product synthesis. *Purr. Appl. Chem.* **1999**, *71*, 979–988. [CrossRef]
12. Spivey, A.C.; Srikaran, R.; Diaper, C.M.; Turner, D.J. Traceless solid phase synthesis of 2-substituted pyrimidines using an "off-The-Shelf" chlorogermane-functionalised resin. *Org. Biomol. Chem.* **2003**, *1*, 1638–1640. [CrossRef]
13. Souza, F.R.; Souza, V.T.; Ratzlaff, V.; Borges, L.P.; Oliveira, M.R.; Bonacorso, H.G.; Zanatta, N.; Martins, M.A.P.; Mello, C.F. Hypothermic and antipyretic effects of 3-methyl- and 3-phenyl-5-hydroxy-5-trichloromethyl-4,5-dihydro-1H-pyrazole-1-carboxyamides in mice. *Eur. J. Pharmacol.* **2002**, *451*, 141–147. [CrossRef]
14. Wang, Y.F.; Izawa, T.; Kobayashi, S.; Ohno, M. Stereocontrolled synthesis of (+)-negamycin from an acyclic homoallylamine by 1,3-asymmetric induction. *J. Amer. Chem. Soc.* **1982**, *104*, 6465–6466. [CrossRef]
15. Zhang, Z.H.; Yin, L.; Wang, Y. A General and Efficient Method for the Preparation of β-Enamino Ketones and Esters Catalyzed by Indium Tribromide. *Adv. Synth. Catal.* **2006**, *348*, 184–190. [CrossRef]
16. Laskar, R.A.; Begum, N.A.; Mir, M.H.; Ali, S.; Khan, A.T. Vanadium (IV) acetylacetonate catalyzed stereoselective synthesis of β-enaminoesters and β-enaminones. *Tetrahedron Lett.* **2013**, *54*, 436–440. [CrossRef]
17. Lenin, R.; Raju, R.M. Lanthanum trichloride: An efficient Lewis acid catalyst for chemo and regioselective enamination of β-dicarbonyl compounds. *Arkivoc* **2007**, *13*, 204–209.
18. Yu, X.; Wang, L.; Feng, X.; Bao, M.; Yamamoto, Y. Copper-Catalyzed aldol-Type addition of ketones to aromatic nitriles: A simple approach to enaminone synthesis. *Chem. Commun.* **2013**, *49*, 2885–2887. [CrossRef]
19. Eshghi, H.; Seyedi, S.M.; Safaei, E.; Vakili, M.; Farhadipour, A.; Bayat-Mokhtari, M. Silica supported $Fe(HSO_4)_3$ as an efficient, heterogeneous and recyclable catalyst for synthesis of β-enaminones and β-enamino esters. *J. Mol. Catal. A Chem.* **2012**, *363*, 430–436. [CrossRef]
20. Bhatte, K.D.; Tambade, P.J.; Dhake, K.P.; Bhanage, B.M. Silver nanoparticles as an efficient, heterogeneous and recyclable catalyst for synthesis of β-enaminones. *Cat. Commun.* **2010**, *11*, 1233–1237. [CrossRef]
21. Rout, L.; Kumar, A.; Dhaka, R.S.; Dash, P. Bimetallic Ag–Cu alloy nanoparticles as a highly active catalyst for the enamination of 1, 3-dicarbonyl compounds. *RSC Adv.* **2016**, *6*, 49923–49940. [CrossRef]
22. Turner, M.J.; McKinnon, J.J.; Wolff, S.K.; Grimwood, D.J.; Spackman, P.R.; Jayatilaka, D.; Spackman, M.A. Crystal Explorer17 (2017) University of Western Australia. Available online: https://crystalexplorer.scb.uwa.edu.au/ (accessed on 7 April 2020).
23. Chen, J.; Zhang, Z.; Liu, S.; Yang, C.; Xia, C. One-Pot tandem synthesis of 2, 3-Unsubstituted indoles, an improved Leimgruber–Batchoindole synthesis. *RSC Adv.* **2014**, *4*, 4672–4675. [CrossRef]
24. Frisch, M.J.; Trucks, G.W.; Schlegel, H.B.; Scuseria, G.E.; Robb, M.A.; Cheeseman, J.R.; Scalmani, G.; Barone, V.; Mennucci, B.; Petersson, G.A.; et al. *GAUSSIAN 09*; Revision A02; Gaussian Inc.: Wallingford, CT, USA, 2009.
25. Reed, A.E.; Curtiss, L.A.; Weinhold, F. Intermolecular interactions from a natural bond orbital, donor-acceptor viewpoint. *Chem. Rev.* **1988**, *88*, 899–926. [CrossRef]
26. Marten, B.; Kim, K.; Cortis, C.; Friesner, R.A.; Murphy, R.B.; Ringnalda, M.N.; Sitkoff, D.; Honig, B. New Model for Calculation of Solvation Free Energies: Correction of Self-Consistent Reaction Field Continuum Dielectric Theory for Short-Range Hydrogen-Bonding Effects. *J. Phys. Chem.* **1996**, *100*, 11765–11775. [CrossRef]

27. Tannor, D.J.; Marten, B.; Murphy, R.; Friesner, R.A.; Sitkoff, D.; Nicholls, A.; Ringnalda, M.; Goddard, W.A.; Honig, B. Accurate first principles calculation of molecular charge distributions and solvation energies from ab initio quantum mechanics and continuum dielectric theory. *J. Am. Chem. Soc.* **1994**, *116*, 11875–11882. [CrossRef]
28. Li, M.; Fang, D.; Geng, F.; Dai, X. Silver-Catalyzed efficient synthesis of enaminones from propargyl alcohols and amines. *Tetrahedron Lett.* **2017**, *58*, 4747–4749. [CrossRef]
29. Foresman, J.B.; Frisch, A. *Exploring Chemistry with Electronic Structure Methods*, 2nd ed.; Gaussian: Pittsburgh, PA, USA, 1996.
30. Chang, R. *Chemistry*, 7th ed.; McGraw-Hill: New York, NY, USA, 2001.
31. Kosar, B.; Albayrak, C. Spectroscopic investigations and quantum chemical computational study of (E)-4-methoxy-2-[(p-tolylimino) methyl] phenol. *Spectrochim. Acta* **2011**, *78*, 160–167. [CrossRef]
32. Koopmans, T.A. Ordering of wave functions and eigenenergies to the individual electrons of an atom. *Physica* **1933**, *1*, 104–113. [CrossRef]
33. Parr, R.G.; Yang, W. *Density-Functional Theory of Atoms and Molecules*; Oxford University Press: New York, NY, USA, 1989.
34. Parr, R.G.; Szentpaly, L.V.; Liu, S. Electrophilicity index. *J. Am. Chem. Soc.* **1999**, *121*, 1922–1924. [CrossRef]
35. Singh, R.N.; Kumar, A.; Tiwari, R.K.; Rawat, P.; Gupta, V.P. A combined experimental and quantum chemical (DFT and AIM) study on molecular structure, spectroscopic properties, NBO and multiple interaction analysis in a novel ethyl 4-[2-(carbamoyl) hydrazinylidene]-3,5-dimethyl-1H-pyrrole-2-carboxylate and its dimer. *J. Mol. Strut.* **2013**, *1035*, 427–440. [CrossRef]
36. Cheeseman, J.R.; Trucks, G.W.; Keith, T.A.; Frisch, M.J. A Comparison of Models for Calculating Nuclear Magnetic Resonance Shielding Tensors. *J. Chem. Phys.* **1996**, *104*, 5497–5509. [CrossRef]